RSC Sustainability

ROYAL SOCIETY OF CHEMISTRY

CRITICAL REVIEW

View Article Online
View Journal | View Issue

Cite this: *RSC Sustainability*, 2025, **3**, 2733

Unlocking the carbon dioxide photoreduction potential of graphene-derived catalysts: mechanisms, product selectivity, and challenges

Manisha Sain, †[a] Debanjali Dey,†[b] Ramkrishna Sen[b] and Shamik Chowdhury *[a]

The escalating concentration of carbon dioxide (CO_2) in the atmosphere necessitates innovative strategies to address global warming and simultaneously harness its potential as a valuable resource. To offset CO_2 emissions, heterogeneous photocatalysis has emerged as an effective technology to photochemically reduce CO_2 into value-added chemicals using specially designed photocatalysts. However, photocatalysts mediating CO_2 reduction often encounter some intrinsic challenges like low specific surface area, inefficient charge separation, narrow visible light absorption, and inadequate stability. Graphene-based materials are widely regarded as a promising solution to address these limitations, offering an enormous specific surface area, excellent electron mobility, and robust chemical stability, which collectively enhance CO_2 conversion efficiency and ensure durable photocatalyst performance. This review delves into the forefront of visible light assisted photocatalytic reduction of CO_2, with a particular focus on graphene-based photocatalysts. The goal is to uncover sustainable solutions that utilize visible light to catalyze the reduction of CO_2, offering an eco-friendly alternative to fossil fuels, while simultaneously acting as a carbon sink by capturing atmospheric CO_2. This review discusses the constraints and challenges of graphene-based composites, encompassing their synthesis techniques and performance efficacy, and provides an outlook on the various product selectivities during CO_2 photoreduction. A brief overview of the potential products obtained from CO_2 photoreduction, with an insight into their plausible mechanism for the production of solar fuel and value-added chemicals, is provided. This timely review, therefore, aspires to expatiate on the recent advances in CO_2 capture and sequestration using graphene-based heterogeneous photocatalysis.

Received 16th January 2025
Accepted 18th May 2025

DOI: 10.1039/d5su00033e

rsc.li/rscsus

Sustainability spotlight

This review underscores the transformative potential of graphene-based photocatalysts for visible light-driven CO_2 reduction, highlighting their role in promoting sustainable solutions for reducing greenhouse gas emissions and producing value-added chemicals. Due to their advantages such as efficient charge separation, broad light absorption, and long-term stability, graphene-based materials offer a promising approach to addressing the current limitations of photocatalytic technologies. The discussed advancements are closely aligned with the UN Sustainable Development Goals (SDGs), particularly SDG 7 (Affordable and Clean Energy), SDG 13 (Climate Action), and SDG 12 (Responsible Consumption and Production). This approach not only drives innovation in renewable energy but also fosters a circular carbon economy, emphasizing environmentally sustainable strategies to combat climate change and support the development of green technologies.

1. Introduction

The recent surge in technological advancements due to rapid industrialization has significantly elevated global energy demands. Fossil fuels remain the primary energy source for the majority of sectors, resulting in a substantial increase in atmospheric carbon dioxide (CO_2) concentrations. Because CO_2 is a major greenhouse gas, urgent measures are imperative to curtail its release into the atmosphere.[1–3] Strategies to stabilize atmospheric CO_2 concentration generally fall into three categories: (a) reducing CO_2 emissions at the source, (b) enhancing CO_2 removal *via* capture and storage, and (c) CO_2 utilization through converting it into valuable chemicals.[4–6] The first strategy emphasizes phasing out fossil fuels and promoting renewable energy sources like solar, hydro, wind, and geothermal power, leading to a substantial reduction in CO_2 emissions from the energy sector.[7,8] The second category involves carbon capture and storage technologies, wherein CO_2 emitted from power plants and industrial processes is captured

[a]*School of Environmental Science and Engineering, Indian Institute of Technology Kharagpur, West Bengal 721302, India. E-mail: shamikc@iitkgp.ac.in*

[b]*Department of Bioscience and Biotechnology, Indian Institute of Technology Kharagpur, West Bengal 721302, India*

† Equal contribution.

and stored in underground geological formations, preventing its release into the atmosphere.[9,10] The third category explores CO_2 reduction into chemicals/fuels, a promising approach in the realm of sustainable and clean energy technologies, especially using solar light as an energy source.[10–12] Such an artificial photosynthesis method harnesses solar energy to transform CO_2 into value-added chemicals or fuels in an aqueous medium, providing a sustainable energy source while contributing to CO_2 emission mitigation.[13,14] However, CO_2 photoreduction remains an evolving technology, with challenges such as higher product yield and scalability still to be addressed.[15] Nevertheless, research and investment in this area contribute to the broader sustainable goals of addressing climate change, mitigating greenhouse gas emissions, and transitioning to a more sustainable and renewable energy-based economy.

Photocatalytic CO_2 reduction has garnered significant scientific attention under the name of artificial photosynthesis.[16–19] Mimicking natural photosynthesis in an artificial system by virtue of photocatalysis implies the usage of earth-abundant semiconductor materials that absorb light in the visible spectrum. Various semiconductor materials, including zinc oxide (ZnO), iron oxide (Fe_2O_3), russellite (Bi_2WO_6), titanium dioxide (TiO_2), graphitic carbon nitride (g-C_3N_4), and cadmium sulphide (CdS), are widely investigated to facilitate photocatalytic CO_2 reduction.[20–30] However, each of them has certain limitations that impel researchers to explore novel, versatile materials with exceptional physicochemical properties.

Graphene has garnered the curiosity of the scientific community due to its exceptional mechanical, optical, electrical, and thermal properties.[31–34] The unique atomic arrangement of graphene in a hexagonal lattice grants it extraordinary properties as depicted in Fig. 1, making it one of the most promising materials of the 21st century. Graphene has high electron mobility and excellent conductivity that facilitates electron transfer through its π-conjugated two-dimensional (2D) structure, thereby improving charge carrier transfer to the photocatalyst surface. The large π-conjugated 2D structure of graphene supports CO_2 activation and destabilization due to π–π conjugate interaction with CO_2.[35,36] Due to these attributes, graphene-based photocatalysts have emerged as promising candidates for the photocatalytic reduction of CO_2. Graphene derivatives and their diverse properties have led to a surge in their usage in technological and scientific areas, as evidenced by the substantial increase in publications on graphene-based photocatalysis.[37–43] To analyze the research trends in graphene-based composites for photocatalytic CO_2 reduction, a Scopus database search was conducted using the keywords "photocatalytic reduction", "graphene", and "CO_2", and the resulting publication data from 2014 to 2024 are presented in Fig. 2a. The current research progress pertaining to graphene evinces that coupling graphene derivatives with suitable semiconductors raises the prospect of fabricating novel multifunctional composite materials for augmenting CO_2 photocatalytic reduction activity. Additionally, there are ample opportunities for ameliorating the performance efficacy of graphene-based composites through proper optimization and tuning of surface chemistry.

In a nutshell, this review aims to summarize CO_2 photocatalytic reduction using graphene-based composites and their probable product formation. To begin with, it briefly iterates the principles and activation mechanism of CO_2 photocatalytic reduction, followed by a concise summary of the fine-tuned and robust graphene-based composites manifesting remarkable CO_2 photoreduction activity. In particular, a clear acumen on the tailored product selectivity during the photocatalytic reduction of CO_2 is provided. Finally, the challenges and future prospects for graphene-based photocatalysts in CO_2 reduction are thoroughly discussed.

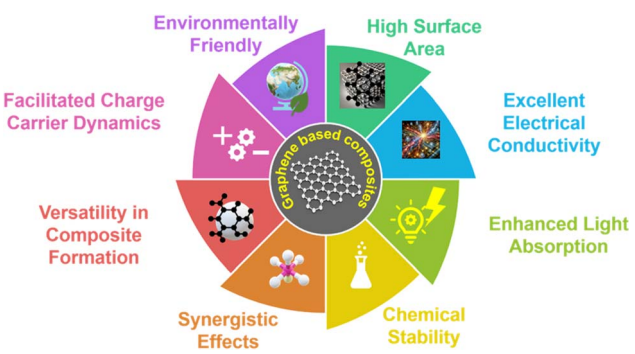

Fig. 1 Advantages of graphene-based composites for photocatalysis.

2. Basic principle and the activation mechanism of CO_2 photocatalytic reduction

The linear structure of the CO_2 molecule, characterized by its chemical inertness and thermodynamic stability, poses a challenge to photocatalytic reduction since it requires high energy input to break the σ and π bonds of O=C=O. The standard Gibbs-free energy (ΔG^0) required for the photocatalytic reduction of CO_2 in an aqueous medium (*i.e.*, water, H_2O) into value-added compounds, including carbon monoxide (CO), methane (CH_4), methanol (CH_3OH), formaldehyde (HCHO), and formic acid (HCOOH) is significantly positive, as depicted in Fig. 2b. This suggests that substantial external energy input is required to convert CO_2 into value-added compounds and fuels. This energy is essential for overcoming reaction barriers, breaking the C=O bond, and facilitating the formation of C–C/C–H bonds, which ultimately result in the desired chemical products.[44]

Furthermore, CO_2 photocatalytic reduction relies on the absorption of photons by semiconductor photocatalysts, leading to the generation of electron–hole pairs. These photoinduced charges thereupon participate in redox reactions with CO_2, driving the conversion of the greenhouse gas into compounds with lower environmental impact.[45] Solar light can serve as the energy source that initiates the photocatalytic reduction of CO_2 into chemicals/fuels through a variety of chemical transformations, utilizing appropriate photocatalysts.

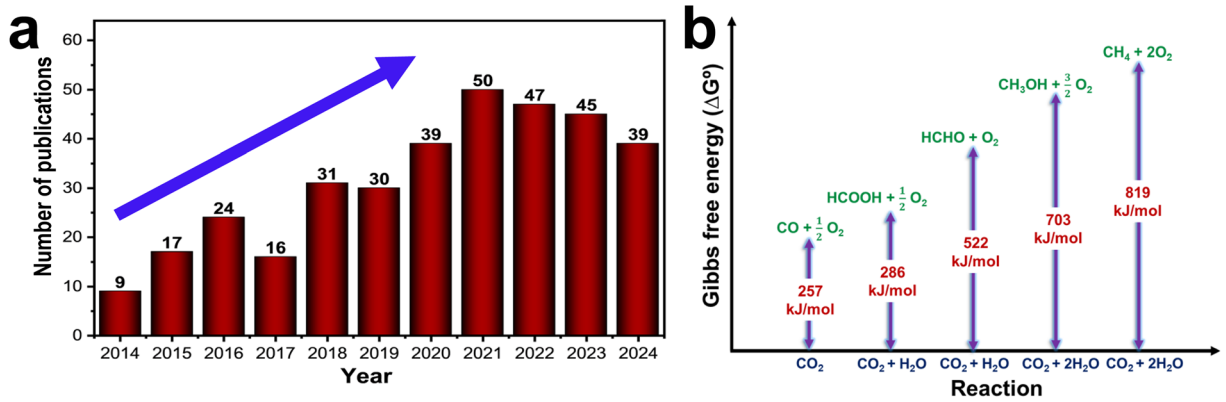

Fig. 2 (a) Publication trends (2014–2024) on Scopus for the keywords "photocatalytic reduction", "graphene", and "CO_2". (b) Gibbs free energy diagram of CO_2 photocatalytic reduction into different value-added products.

The photogenerated charge carriers drift to the active sites on the photocatalyst surface, where holes oxidize H_2O into O_2 thereby liberating H^+ that further assists in electron-mediated reduction of CO_2 *via* a series of reactions (Fig. 3a). However, volumetric or surface recombination of electrons and holes during this process diminishes the photocatalytic reduction efficiency.[46,47] Effective electron–hole separation, critical for CO_2 photocatalytic reduction, can be achieved using nanostructured photocatalysts such as nanorods, nanobelts, nanotubes, and various types of junctions.[48–51]

To escalate the CO_2 reduction efficiency, the reactivity of CO_2 can be increased through various activation mechanisms. Stable CO_2 molecule activation can be achieved through any of the five modes: (a) bending of linear arrangement of the CO_2 molecule (O–C–O) with attachment of the O atom, (b) at least one C–O bond elongation or both, (c) charge (electron) transfer to CO_2 due to polarization of charges on C and O atoms, (d) hydride transfer, and (e) charge redistribution.[52]

Typically, the activation of the CO_2 molecule over heterogeneous catalysts entails a charge transfer (mode c) from the catalyst to the molecule. This transfer elongates the C–O bond length and reduces the O–C–O bond angle (modes a and b).[53,54] The activation of CO_2 at the molecular level occurs due to a partial transfer of electrons into the lowest unoccupied molecular orbital (LUMO).[55] The bending of CO_2 results in a notable reduction of its energy of the LUMO and enhances the electron density of the carbon associated with it, thereby promoting the transfer of an electron to the molecule. Consequently, the bending results in the C–O bond weakening when compared to its linear configuration. This could result in the dissociation of CO_2 on the catalyst surface into CO and O species. These characteristics improve the capacity for CO_2 reduction through electron acceptance.

At the molecular level, activation of stable CO_2 molecules for photocatalytic reduction involves an electron transfer, which initiates multistep chemical reactions on the surface of the photocatalyst. Upon excitation, an electron is transferred from the highest occupied molecular orbital (HOMO) to the LUMO of CO_2, resulting in the formation of the surface-bound CO_2 radical anion ($CO_2^{\bullet-}$).[55] The bent structure of the CO_2 molecule, because of electron transfer from the photocatalyst to the π^* antibonding molecular orbital of CO_2, activates the CO_2 molecule for photocatalytic reduction. However, experimental evidence through scanning tunnelling electron microscopy indicates that a single electron transfer to CO_2 in the gaseous phase is thermodynamically unfavorable, as this creates

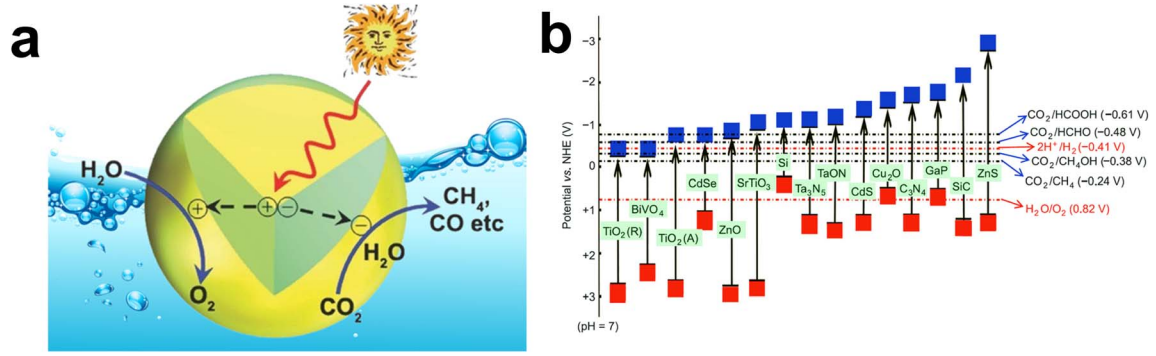

Fig. 3 (a) Schematic of the photocatalytic reduction of CO_2 in an aqueous medium over a graphene-based photocatalyst. Reproduced with permission from ref. 34, copyright 2014, Wiley. (b) Redox potential and band position of different semiconductors for CO_2 reduction into value-added products in aqueous medium. Reproduced with permission from ref. 45, copyright 2014, Springer Nature.

a negative redox potential in the LUMO of CO_2 ($CO_2 + e^- \rightarrow CO_2^{\bullet -}$, $E^0 = -1.9$ V *vs.* NHE, pH = 7).[56] The type of product formation depends on the number of electrons participating in chemical reactions, leading to the production of CO ($2e^-$), HCHO ($4e^-$), CH_3OH ($6e^-$), and CH_4 ($8e^-$).[57] Product selectivity in CO_2 photocatalytic reduction is one of the significant concerns that may vary according to changes in reaction conditions, photocatalyst selection, and thermodynamic reduction potential. The redox potential (E^0) of different products with different semiconductors for CO_2 reduction is shown in Fig. 3b.[58] Table 1 outlines the potential chemical reactions and corresponding E^0 values for CO_2 photocatalytic reduction, highlighting the desired products formed under pH 7 conditions.[58–62]

Surface functional groups on graphene-derived materials, especially hydroxyl, epoxy, and carboxyl groups, play a central role in CO_2 adsorption and activation during photocatalysis. These functionalities create localized polar sites that enhance CO_2 chemisorption through hydrogen bonding and dipole–quadrupole interactions. Once adsorbed, the linear CO_2 molecule undergoes structural distortion into a bent configuration, forming a $CO_2^{\bullet -}$ radical intermediate, a critical step for initiating reduction reactions. These surface interactions not only reduce the energy barrier for activation but also influence the selectivity of photogenerated electrons toward specific reduction pathways, such as CO, CH_4, or CH_3OH production.

Furthermore, heteroatom doping (*e.g.*, N, S, or B) into the graphene lattice introduces additional active sites with modified electronic structures, improving the overlap between the conduction band of the photocatalyst and the LUMO of CO_2. For instance, nitrogen-doped graphene materials have been shown to facilitate better CO_2 activation due to the lone-pair electrons on pyridinic and graphitic nitrogen, which act as coordination centers and enhance electron transfer to CO_2.[55,63] Experimental studies have demonstrated that the presence of carboxyl and hydroxyl groups correlates with increased photocatalytic efficiency, especially in CO and HCOOH production pathways.[64] Such functionalization strategies are increasingly employed to enhance charge carrier separation, as supported by both theoretical and experimental investigations.[65,66]

Table 1 Redox potential of the reactions involved in the CO_2 photocatalytic reduction reaction in aqueous medium ($E°$ in V *vs.* normal hydrogen electrode (NHE), pH = 7, temperature = 27 °C, pressure = 1 atm)

Product	Reaction	$E°$ (V)
CO_2 radical anion	$CO_2 + e^- \rightarrow CO_2^{\bullet -}$	−1.90
Formic acid	$CO_2 + 2H^+ + 2e^- \rightarrow HCOOH$	−0.61
Carbon mono-oxide	$CO_2 + 2H^+ + 2e^- \rightarrow CO + H_2O$	−0.53
Formaldehyde	$CO_2 + 4H^+ + 4e^- \rightarrow HCHO + H_2O$	−0.48
Methanol	$CO_2 + 6H^+ + 6e^- \rightarrow CH_3OH + H_2O$	−0.38
Ethane	$2CO_2 + 14H^+ + 14e^- \rightarrow C_2H_6 + 4H_2O$	−0.27
Methane	$CO_2 + 8H^+ + 8e^- \rightarrow CH_4 + 2H_2O$	−0.24
Oxygen	$2H_2O + 4h^+ \rightarrow O_2 + 4H^+$	0.81
Hydrogen	$2H^+ + 2e^- \rightarrow H_2$	−0.41
Hydroxyl radical	$H_2O + h^+ \rightarrow H^+ + {}^{\bullet}OH$	2.32

3. Graphene-derived photocatalysts for CO_2 reduction

In recent decades, several strategies have been developed to improve the semiconductor performance for CO_2 photocatalytic reduction under visible light. Approaches to optimize the bandgap include doping, altering surface properties, and dye sensitization.[67–69] Additionally, various junctions, including heterojunctions, homojunctions, and Schottky junctions, have been utilized to facilitate charge separation and transport for CO_2 photocatalytic reduction.[70] Graphene plays a pivotal role in this, as it efficiently absorbs a broad spectrum of light, including visible and ultraviolet (UV) wavelengths,[71] improving solar light utilization and making the process more energy efficient. The surface of graphene provides numerous active sites that can support or anchor semiconducting catalytic species, typically non-metal or metal oxide nanoparticles, significantly enhancing the overall CO_2 photocatalytic reduction efficiency. Furthermore, the high electrical conductivity and huge specific surface area of graphene enable rapid charge carrier separation and transfer to active sites, driving the CO_2 reduction reactions on graphene-based photocatalysts.[47,72,73] In recent advancements, researchers have combined graphene with other nanomaterials or co-catalysts to form hybrid structures that exhibit synergistic effects, resulting in improved photocatalytic activity and selectivity for CO_2 reduction. Various types of graphene derivatives have been reported in the literature, such as graphene oxide (GO), graphene nanocrystals, and graphene-based composites that offer a promising route for converting CO_2 emissions into valuable products, contributing to carbon capture and utilization. Therefore, it is anticipated that graphene-based composites will diversify opportunities and provide exceptional properties to photoactive materials, thereby advancing value-added chemical production by CO_2 photocatalytic reduction using solar energy. Table 2 provides a summary of the various graphene-based composites employed for CO_2 photocatalytic reduction.

3.1. Graphene–inorganic composites

Graphene-based inorganic composites are formed by integrating graphene or its derivatives with inorganic materials, such as metal oxides or metal nanoparticles, in order to improve their photocatalytic performance. In particular, these composites have shown promising results in improving light absorption capacity, charge carrier separation, and catalytic activity. Additionally, the large specific surface area of graphene provides exceptional support for catalysts. The presence of graphene increases the adsorption of CO_2 on the catalyst surface along with the enhancement of electron–hole separation in the composite photocatalyst.[93] Although TiO_2 is widely used for driving photocatalytic reactions, it faces challenges such as a wide bandgap energy of 3.2 eV (limiting excitation to the UV range) and rapid electron–hole recombination.[94] Modification of TiO_2 through graphene incorporation addresses these challenges by altering the bandgap, minimizing charge recombination, increasing specific surface area, and enhancing

Table 2 Graphene-derived photocatalysts for solar fuel production *via* CO_2 photocatalytic reduction.

Photocatalyst	Synthesis method	Light source (wavelength)	Product	Reference
Graphene-g-C_3N_4	Impregnation-thermal reduction process	Daylight bulb, 15 W	Methane (5.87 μmol g^{-1})	26
Modified graphene oxide (GO)	Improved Hummer's method	Halogen lamp, 300 W	Methanol (0.172 μmol g_{cat}^{-1} h^{-1}	74
GO-tungsten trioxide	Facile hydrothermal method (180 °C, 12 h)	Xenon lamp, 300 W	Methane (0.11 μmol h^{-1})	75
Platinum modified rGO with TiO_2 nanotubes	Hydrothermal synthesis (120 °C, 24 h)	Xenon lamp, 300 W	Alcohol and carboxylic acid (1130 nmol h^{-1} cm^{-2}	76
GO decorated with copper nanoparticles	Rapid microwave process (one-pot)	2 h of visible light irradiation	Acetaldehyde 3.88 μmol g_{cat}^{-1} h^{-1} & methanol 2.94 μmol g_{cat}^{-1} h^{-1}	77
Noble metal Ag, Au, Pd, & Pt modified rGO/TiO_2	Polyol process	Xenon arc lamp, 500 W	Methane (1.70 μmol g_{cat}^{-1}) in 6 h	78
Graphene derivative TiO_2	Liquid phase deposition method	Mercury vapour lamp	Methanol (47 μmol g^{-1} h^{-1}), ethanol (144.7 μmol g^{-1} h^{-1})	79
rGO-copper oxide		Visible light (λ > 420 nm)	Methanol (max 1225 μmol g_{cat}^{-1})	80
Graphene supported TiO_2 nanocrystal −001/101	Solvothermal method	Xenon arc lamp, 300 W	Carbon monooxide (70.8 μmol g^{-1} h^{-1})	81
CuO/Cu_2O nanowire with rGO graft	Thermal oxidation method	Xenon arc lamp, 500 W	Carbon monoxide (0.31 and 0.20 μmol cm^{-2})	82
GO-supported oxygen-TiO_2	Precipitation method followed by the impregnation method	Xenon arc lamp, 500 W	Methane (3.45 μmol g_{cat}^{-1})	83
GO/modified cobalt		Xenon lamp, 300 W (λ > 420 nm)	Formic acid (96.49 μmol for 2 h)	84
Blue titania/graphene/platinum		Xenon lamp, 300 W (λ > 420 nm)	Methane (259 μmol g^{-1} h^{-1}), ethane (77 μmol g^{-1} h^{-1})	85
α-Ferric oxide-zinc oxide/rGO	Electrochemical process	Xenon lamp, 300 W (λ > 420 nm)	Methanol (5.3 μmol g^{-1} in 3 h)	86
Graphene-chlorophyll copper		Visible light	Ethane (68.23 μmol m^{-2} h^{-1})	87
In_2O_3/rGO		Mercury lamp, 250 W (λ, 400–700 nm)	Methane (953.72 μmol g^{-1})	88
p-type nickel oxide/n-type ceric oxide/rGO	Hydrothermal process	Xenon lamp, 300 W	Formaldehyde (421.09 μmol g^{-1} h^{-1})	89
Poly(3-hexylthiophene-2,5-diyl) (P3HT)/GO hybrid	Mini-emulsion method	Halogen lamp 300 W	Methanol and acetaldehyde	90
g-C_3N_4/rGO	Hydrothermal method	Xenon lamp, 300 W (PLS-SXE300D), AM 1.5G filter	Methanol (114 μmol g^{-1} h^{-1}), H_2 (68 μmol g^{-1} h^{-1})	41
GO/copper oxide/copper organic frame	Hydrothermal method	Xenon lamp150 W, AM 1.5 filter (100 mW cm^{-2})	Alcohol (methanol, ethanol, propanol) (2217 nmol h^{-1} cm^{-2})	91
Gold/TiO_2/N-graphene	Hydrothermal method	Xenon lamp, 300 W (λ > 420 nm)	Methane (742.39 μmol g^{-1} h^{-1})	92

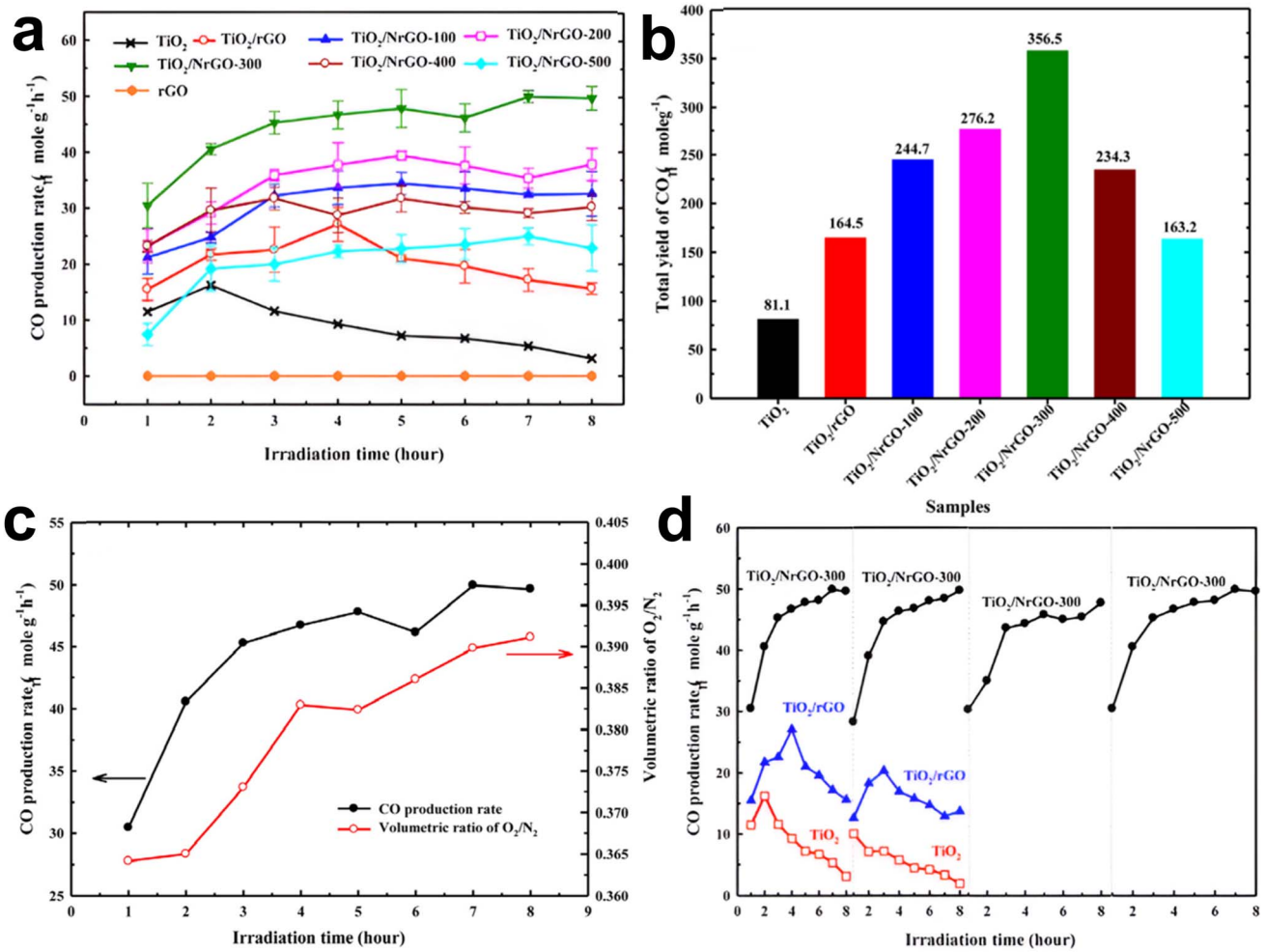

Fig. 4 (a) CO production rate *via* photocatalytic reduction of CO_2 with respect to irradiation time, and (b) total yield of CO under visible light irradiation using rGO, TiO_2 and TiO_2/NrGO-X. (c) Rate of CO production and the volumetric ratio of O_2/N_2 over TiO_2/NrGO-300. (d) Recyclability test over TiO_2/NrGO-300 for the CO_2 photocatalytic reduction rate through four consecutive cycles. Reproduced with permission from ref. 80, copyright 2017, Elsevier Ltd.

photocatalytic efficiency in the visible light range.[95] In a notable study, a TiO_2/nitrogen-doped reduced graphene oxide (rGO) composite (TiO_2/NrGO) was synthesized *via* a one-step hydrothermal method for CO_2 photocatalytic reduction.[96] The incorporation of nitrogen (N_2) dopants produced a synergistic effect, improving CO_2 adsorption on the catalyst surface and facilitating the transfer of photogenerated electrons. Furthermore, this study focused on CO_2 reduction at a gas–solid interface, where CO was found to be the primary product in the flow reactor system. This is because CO requires fewer electrons and protons and is kinetically favored for production. The absence of CH_4 in this study may be due to the fact that the photoreduction of CO_2 to CH_4 demands more electrons and protons, making its formation more challenging than CO. Notably, in addition to quaternary-N moieties functioning as electron-transfer mediator, both pyridinic-N and pyrrolic-N motifs serve as active sites for CO_2 reduction, enhancing the interfacial photocatalytic activity. As a result, the modified catalyst exhibited a significant total CO production yield of 356.5 μmol g^{-1}, which is a 4.4 times increase compared to pure TiO_2 (81.1 μmol g^{-1}) and a 2.2 fold increase over TiO_2/reduced graphene oxide (TiO_2/rGO) (160.5 μmol g^{-1}) as shown in Fig. 4a and b. Additionally, Fig. 4c and d show the CO production rate with respect to the O_2/N_2 volume ratio and the CO_2 photocatalytic reduction rate over recycled TiO_2/NrGO-300, respectively.[96] It is noteworthy to mention that doping of noble metal nanoparticles into rGO/TiO_2 (GT) resulted in an enhanced photoactivity towards CO_2 reduction to CH_4.[78] Thus, a set of noble metal (NM)-doped GT nanocomposites, including platinum (Pt), palladium (Pd), silver (Ag), and gold (Au), were successfully prepared using a simple polyol method. Among the NM–GT samples, the Pt–GT nanocomposite exhibited the highest photocatalytic activity, achieving a total CH_4 yield of 1.70 μmol g_{cat}^{-1} after 6 h of light irradiation. This is attributed to the strong dependence of the photonic efficiency of NM-GT on the electron affinity and work function of the metal, which favors its contact with TiO_2. Pt has a higher work function (−5.65 eV) compared to Au (−5.1 eV), Ag (−4.7 eV), and Pd (−5.2 eV).

Consequently, the photogenerated electrons can transfer more efficiently from TiO_2 to Pt nanoparticles, while the reverse process is significantly hindered. Furthermore, the Pt nanoparticles significantly contributed to the CO_2 reduction potential by enhancing charge separation and transfer while extending the absorption band into the visible light spectrum.[78] In a subsequent study by Deerattrakul and coworkers, Cu–Zn/rGO was prepared with varying weight percentages of Cu–Zn, using an equimolar ratio of Cu and Zn on an rGO support through the incipient wetness impregnation method.[97] The rGO-supported nanosheets significantly improved the catalytic performance and facilitated the dispersion of Cu–Zn bimetallic particles. The catalyst achieved a CH_3OH production rate of 424 mg CH_3OH g_{cat}^{-1} h^{-1}, indicating its potential for practical CO_2 conversion to CH_3OH.[97] In another study, the integration of β-Ga_2O_3 nanorods with rGO nanosheets presented a highly efficient catalytic architecture. The innovative β-Ga_2O_3–rGO composite demonstrated a significant enhancement in CO production yield along with an impressive 98% CO selectivity. This exceptional performance highlights the substantial enhancements achieved through the innovative rGO integration approach.[98]

Researchers are actively investigating novel combinations of graphene with various inorganic materials, whereby tailoring the structural and electronic properties of composite materials may aim to improve CO_2 adsorption, electron transfer, and selectivity for desired products, such as fuels and chemicals.

3.2. Graphene–2D material composites

The integration of graphene with other 2D materials takes advantage of the complementary properties of both graphene and the selected 2D material to improve the efficiency and selectivity of the CO_2 photocatalytic reduction process. Various 2D materials, such as g-C_3N_4, molybdenum disulfide (MoS_2), and tin disulfide (SnS_2), have been explored in combination with graphene.[36,41,99–103]

For instance, g-C_3N_4, a metal-free semiconductor, with a medium bandgap energy, is widely employed in the realm of photocatalysis. Both g-C_3N_4 and graphene have sp^2 hybridized π bonds that aid in π–π interaction among them and also destabilize CO_2 molecules because of delocalized π-conjugate binding with CO_2.[26,104] When g-C_3N_4 is combined with graphene, the composite can provide enhanced light absorption and charge transport properties, making it suitable for CO_2 photocatalytic reduction. In a recent study, a composite of g-C_3N_4 with graphene was synthesized for CH_3OH production *via* CO_2 photocatalytic reduction.[41] Herein, g-C_3N_4 was synthesized using the co-polymerization method by annealing guanidine carbonate (G) and ammonium thiocyanate (A) together at 5 wt% each, termed G_5A_5. Initially, hydrogen (H_2) was the sole product obtained when G_5A_5 (as-synthesized g-C_3N_4 with the lowest bandgap) was used as the photocatalyst, while the G_5A_5/rGO composites produced both CH_3OH and H_2. Thus, it is evident that the addition of rGO to G_5A_5 facilitated the formation of CH_3OH.[41] Furthermore, the experimental results suggest that the conduction band of G_5A_5 likely lies below the CO_2/CH_3OH reduction potential, which thermodynamically prevents CO_2 from being reduced to CH_3OH. However, incorporating rGO with semiconductors (like g-C_3N_4) causes an upward shift in the G_5A_5 bands due to electron transfer from rGO. This band shifting allows the band edges to align with the CO_2/CH_3OH and H_2O/O_2 redox potentials, enabling the generation of CH_3OH. Fig. 5a and b illustrate H_2 and CH_3OH yields on employing a series of composites at different concentrations under optimal conditions.[41] The composite giving the maximum yield is identified as the combination of g-C_3N_4 and rGO at a 5 wt% concentration, denoted as G_5A_5/rGO_5. Fig. 5c depicts H_2 and CH_3OH evolution using G_5A_5/rGO_5 at a concentration of 3 mg mL^{-1} under 12 h of solar light. The results showed that over six effective cycles, nearly 114 μmol g^{-1} h^{-1} of CH_3OH and 68 μmol g^{-1} h^{-1} of H_2 were collected.[41]

MoS_2, a widely studied 2D semiconductor known for its exceptional catalytic properties, shows enhanced performance when combined with graphene. This composite effectively facilitates charge separation and has demonstrated good stability and reusability across multiple photocatalytic cycles.[102,105–107] The combination has exhibited promising results in augmenting the production of value-added chemicals and fuels from CO_2 photocatalytic reduction. To this end, a highly efficient, metal-free, and stable photocatalyst with a hierarchical porous structure was developed using a one-pot hydrothermal method as depicted in Fig. 6a.[105] The

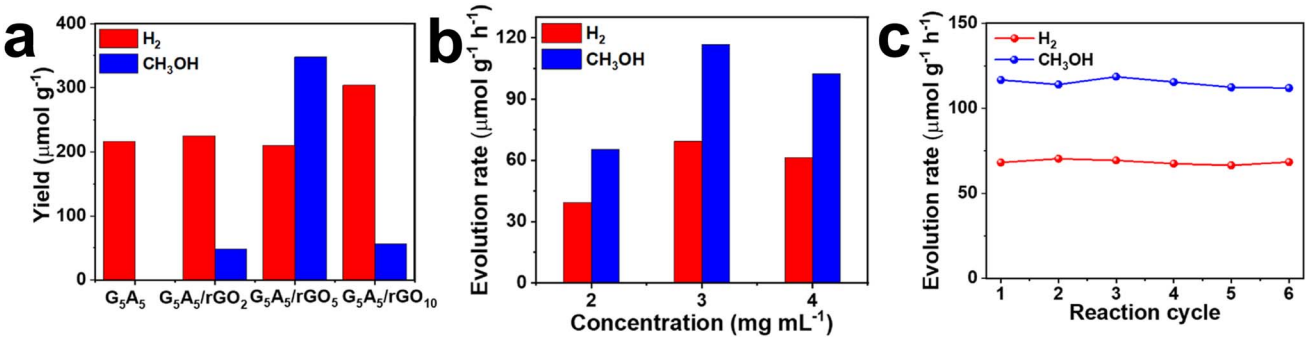

Fig. 5 (a) Hydrogen and methanol yields using G_5A_5 and its rGO composites, (b) hydrogen and methanol yields at varying concentrations using G_5A_5 and its rGO composites, and (c) hydrogen and methanol evolution rates using G_5A_5/rGO_5 (3 mg mL^{-1}) under 12 h solar light. Reproduced with permission from ref. 74, copyright 2022, Elsevier Ltd.

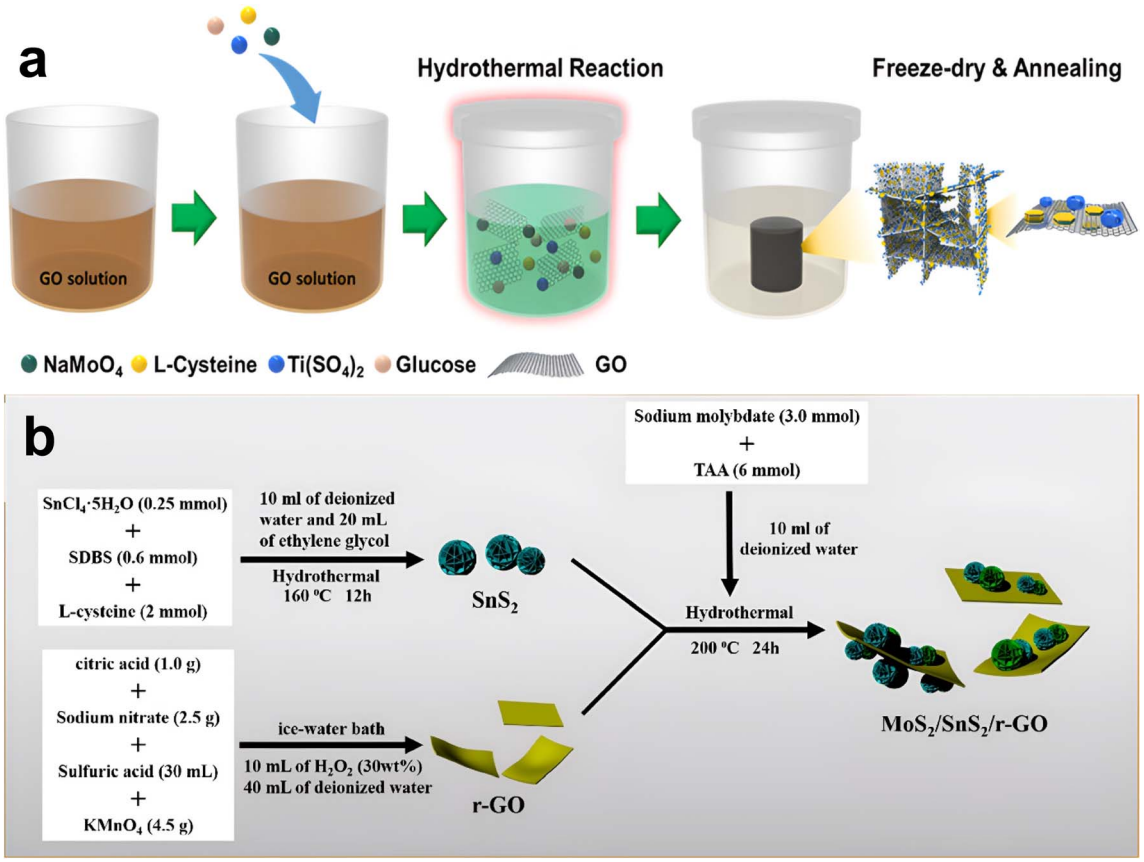

Fig. 6 (a) Illustration of the synthesis approach of a TiO_2–graphene–MoS_2 composite. Reproduced with permission from ref. 89, copyright 2018, the American Chemical Society. (b) Schematic of the MoS_2/SnS_2/r-GO fabrication procedure. Reproduced with permission from ref. 85, copyright 2019, the American Chemical Society.

composite, denoted as TGM, comprised TiO_2 (T), graphene (G), and MoS_2 (M) nanosheets, which contributed to the formation of its porous architecture. MoS_2, known for its robustness and layer-dependent catalytic activity, acted as a co-catalyst, whereas graphene served as an electron channel component. This assembly provided a large specific surface area and expedited efficient mass transfer through its randomly distributed porous backbone. The electron transfer from TiO_2 through graphene to the few-layered MoS_2 effectively reduced charge recombination and boosted the CO_2 reduction potential. As a result, the composite achieved a remarkable CO production rate of 92.33 μmol CO g^{-1} h^{-1}.[105] In another study, a ternary composite of MoS_2, g-C_3N_4, and graphene was synthesized *via* an ultrasonication-mediated calcination process by Otgonbayar and co-workers.[100] The investigation revealed a positive change in the electronic structure without altering the internal crystal and electronic structures of individual nanocomposites. The application of an aqueous solvent containing a basic salt and a donor scavenger enhanced the photocatalytic CO_2 reduction through the type-II heterojunction. This facilitates the efficient supply of a large number of electrons and hydrated CO_2 molecules necessary for the complex reduction reaction of CO_2 to alcohol.[100]

Another interesting 2D semiconductor with a layered structure, *i.e.*, SnS_2, possesses a favorable conduction band position and an optimal bandgap, enhancing its ability to efficiently reduce CO_2 and improve sunlight absorption. A 3D MoS_2/SnS_2/rGO nanocomposite, synthesized *via* a solvothermal method (Fig. 6b), demonstrated effective CO_2 photoreduction under UV light.[101] The distinctive structure of metal sulfides within the same family enhances defect formation and minimizes electron transport barriers, facilitating efficient electron transfer at the interface through electron tunneling and offering more active sites for CO_2 reduction. The constructed S–C–S heterojunction exhibits a multilevel electron transport mechanism and synergistic interactions, increasing the potential for producing a higher yield of organic fuels. Thus, the unique design of the Z-type heterojunction (Fig. 7) provided lower diffusion resistance and faster ion diffusion channels, thereby forming CO and CH_4 at an impressive rate of 68.63 μmol g^{-1} h^{-1} and 50.55 μmol g^{-1} h^{-1}, respectively.[101]

Recently, a novel composite consisting of porous carbon-doped hexagonal boron nitride nanoribbons (c-BNNR) combined with photosensitizing graphene quantum dots (GQDs) was developed.[108] The presence of a 0D/1D interaction between GQDs and c-BNNR facilitates electron transfer from GQDs to the c-BNNR surface. Notably, the introduction of GQDs effectively reduced electron–hole recombination, enhanced the generation of surface-active electrons, and selectively reduced CO_2 to CO (123.81 μmol g^{-1}). The improved stability and faster

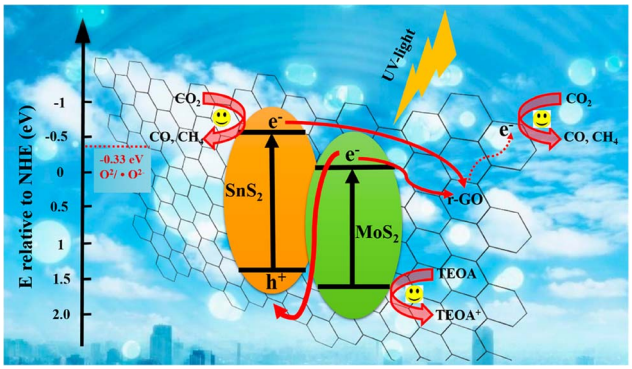

Fig. 7 A plausible mechanism of the energy band structure and charge separation over MoS_2/SnS_2/r-GO during photocatalytic reduction of CO_2. Reproduced with permission from ref. 85, copyright 2019, the American Chemical Society.

electron migration kinetics, enabled by the addition of GQDs, significantly enhanced the CO_2 reduction efficiency of the nanocomposite.[108] Interestingly, a graphene nanoflake (GNF)-decorated zeolitic imidazole framework (ZIF-67), denoted as GNF(X)/ZIF-67, has been synthesized to enhance the efficiency of visible light-driven photocatalytic CO_2 reduction. The composite demonstrated an impressive performance, achieving a CH_3OH production rate of 50.93 μmol g^{-1} and an ethanol (C_2H_5OH) production rate of 33.97 μmol g^{-1} after 8 h of visible light irradiation. These results significantly surpass the performance of pure ZIF-67, thereby serving as a testament to highlight the efficacy of GNF decoration in boosting photocatalytic activity.[109]

The selection of a 2D material to pair with graphene is guided by several factors, such as the specific target reaction, the required photocatalytic properties (*e.g.*, bandgap alignment and charge transfer efficiency), and the feasibility of synthesis techniques. Additionally, considerations like the stability, scalability, and environmental compatibility of the materials play a critical role. Researchers are continuously exploring diverse combinations of graphene with 2D materials to enhance the efficiency, selectivity, and durability of these composites for CO_2 photocatalytic reduction, aiming to maximize the production of value-added chemicals and sustainable fuels.

3.3. Graphene–polymer composites

Graphene–polymer composites have been extensively explored to harness solar energy for CO_2 photocatalytic reduction to chemicals/fuels. Various polymers have been employed in conjunction with graphene, each offering unique properties to enhance the overall performance of the composite in this process. Commonly used polymers with graphene for CO_2 photocatalytic reduction include polypyrrole, poly(3-hexylthiophene) (P3HT), poly(3,4-ethylenedioxythiophene) (PEDOT), poly(ethylene oxide) (PEO), poly(vinyl alcohol) (PVA), poly(4-vinylpyridine) (P4VP), polyaniline, and polyimide.

For instance, a composite of rGO and MoS_2 with varying concentrations of polypyrrole, exhibited enhanced photocatalytic performance for CO_2 reduction in aqueous media under simulated sunlight.[110] This composite demonstrated significant production rates of CH_4 (1.5 μmol g^{-1} h^{-1}), CO (3.95 μmol g^{-1} h^{-1}) and H_2 (4.19 μmol g^{-1} h^{-1}). The polymerization of the composite effectively facilitated charge transfer, light absorption, CO_2 adsorption, and minimized charge carrier recombination due to synergistic effects.[110] Additionally, P3HT is highly favored as a polymeric donor material due to its excellent electrical conductivity and solvent solubility. When integrated with graphene, it improves carrier mobility, conductivity, and hole collection, whereas reducing the bandgap with increasing graphene content.[111] Similar to P3HT, PEDOT is another conjugated polymer that can be incorporated with graphene to facilitate the production of value-added chemicals through CO_2 photocatalytic reduction. PEDOT is known for its high electrical conductivity and stability, which are beneficial for enhancing the performance and durability of the composite.[112] Other polymers, such as PVA, a biocompatible and water-soluble polymer, have been used with graphene in aqueous CO_2 photocatalytic reduction studies. The hydrophilic nature and film-forming properties of PVA make it suitable for such applications.[113,114] Additionally, polyaniline, recognized for its conductive and redox properties, has been shown to synergistically improve charge transfer, light absorption, and catalytic activity in graphene-polyaniline nanocomposites, contributing to more effective CO_2 reduction. For example, Liu and colleagues synthesized a composite of ZnO, GO, and polyaniline for efficient conversion of CH_4 into CH_3OH and HCOOH. This transformation of gaseous fuel into liquid chemicals is advantageous due to the ease of storage and transportation.[115] Furthermore, polyimide, a high-temperature-resistant polymer, demonstrated exceptional performance when combined with graphene in a composite featuring silver chromate and N-rGO, achieving a CO_2 photocatalytic reduction rate of 352.1 μmol g_{cat}^{-1} h^{-1}. The hetero-linkage structure between silver chromate and polyimide created a Z-scheme heterojunction, enhancing light absorption and overall photocatalytic efficiency. Moreover, the presence of pyridinic-N, serving as a unique selective site, facilitated the generation of CO. This feature lowered the free energy barrier for the potential-limiting step, further enhancing the overall efficiency of the photocatalytic process.[116]

The aforementioned examples represent a subset of the polymers explored, and the selection depends on the specific application, environmental conditions, and desired properties of the graphene–polymer composite. Researchers must continue to explore new polymers and optimize existing ones to improve the performance and efficiency of CO_2 photocatalytic reduction systems for sustainable chemical/fuel production.

3.4. Long-term performance and cycling stability of graphene-integrated composites

Long-term cycling tests reveal that, with a robust composite design, graphene-derived photocatalysts can sustain activity over extended operation. For instance, a TiO_2/3D-graphene–MoS_2 composite preserved over 80% of its initial CO_2 to CH_4 conversion rate after 15 consecutive 3 h runs (~45 h total), and

a WSe_2–graphene nanocomposite exhibited negligible loss in methanol yield across six 48 h irradiation cycles (~288 h cumulative).[105,117] Deactivation was primarily attributed to photochemical deoxygenation of GO, defect-mediated photocorrosion of the hybrid interface, and accumulation of carbonaceous residues. Furthermore, a novel N-doped GO–wrapped TiO_2 nanotube catalyst retained over 90% of its initial CH_4 yield throughout a continuous 35 h run. Similarly, CoO/rGO hybrids retained consistent CO evolution across six 24 h cycling tests.[118] These studies confirm that with appropriate composite design and mitigation strategies, graphene-derived materials can achieve day-long photoreduction stability. However, pilot-scale continuous-flow demonstrations remain to be developed. These findings underscore both the promise and the remaining challenges in achieving day-long operational durability under solar-driven conditions.

4. Product selectivity during CO_2 photocatalytic reduction and analysis

The photocatalytic reduction of CO_2 yields major gaseous products, primarily CH_4 and CO, with the presence of H_2O leading to the production of H_2 and O_2 as H_2O splitting byproducts.[92,119–121] In an aqueous environment, a significant challenge lies in product selectivity, particularly as H_2, a major competitor in H_2O splitting, diminishes the selectivity and efficiency of chemical/fuel production during photocatalytic reduction, thereby efforts to suppress H_2 evolution reaction are

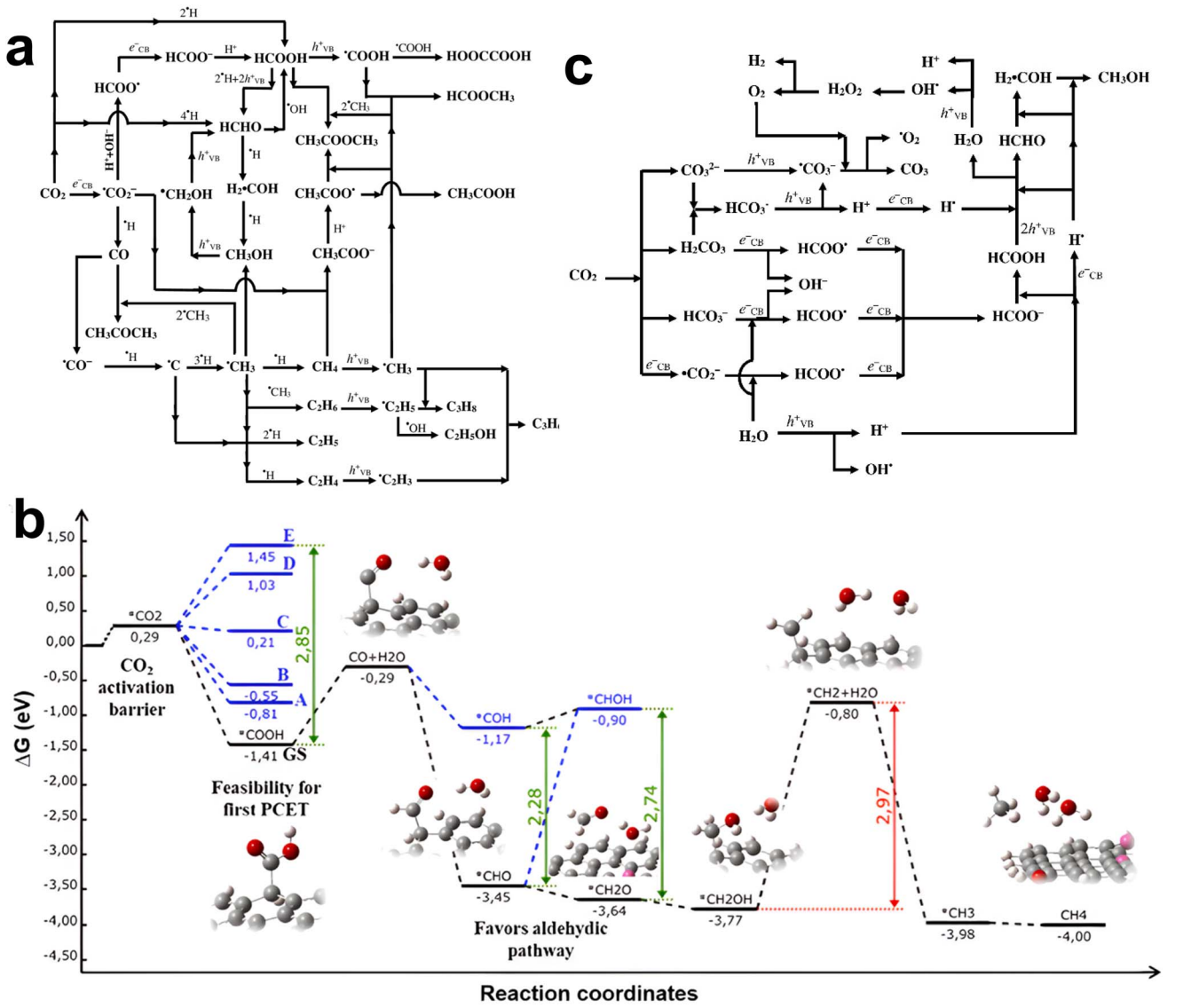

Fig. 8 (a) General pathway for CO_2 photocatalytic reduction in the presence of a mixture of reductants. Reproduced with permission from ref. 105, copyright 2016, Elsevier Ltd. (b) Gibbs free energy (ΔG) diagram for CO_2 reduction into CH_4 and CO on a Au–TiO_2 decorated nitrogen-doped graphene photocatalyst, along with intermediate product adsorption configuration. Reproduced with permission from ref. 76, copyright 2022, Elsevier Ltd. (c) Possible pathways for the production of methanol during photocatalytic reduction of CO_2 in aqueous media. Reproduced with permission from ref. 105, copyright 2016, Elsevier Ltd.

necessary. Coupling CO_2 photocatalytic reduction with H_2O splitting reactions in an aqueous medium helps identify the rate-determining step, contributing to enhanced selectivity and efficiency.[58] A study demonstrated the effectiveness of binary co-catalysts designed to selectively reduce CO_2 in the presence of H_2O. The core–shell-structured Pt@Cu_2O cocatalyst with TiO_2 can effectively suppress the reduction of H_2O to H_2, while significantly promoting the selective reduction of CO_2 to CO and CH_4. The selectivity for CO_2 reduction achieved an impressive 85%.[122]

The product selectivity in CO_2 photocatalytic reduction is intricately linked to its complex hydrogenation and deoxygenation processes. Karamian and Sharifnia have outlined a general pathway for CO_2 photocatalytic reduction reaction, emphasizing the formation of various oxidizing species and the reduction of CO_2 by different reductants such as H_2O, H_2, CH_3OH, and CH_4.[123] The choice of reductant significantly affects the product formation, as can be seen in Fig. 8a. In most instances, CO is the primary product, with subsequent potential products including CH_4 and other hydrocarbons such as acetic acid, HCOOH, CH_3OH, C_2H_5OH, and acetaldehyde (CH_3CHO).[123] Achieving high product selectivity is essential for maximizing target yield in CO_2 photocatalytic reduction, as low selectivity leads to multiple byproducts, complicating product separation processes. The potential products formed during CO_2 photocatalytic reduction are outlined below, with the corresponding reactions responsible for their formation detailed in Table 1. While gaseous phase products are typically analyzed using a gas chromatograph equipped with flame ionization and thermal conductivity detectors, products in the liquid phase, such as alcohols, are detected through direct injection of liquid or heating gasification.[124]

4.1. Methane production

CH_4 stands out as a prominent gaseous product in the realm of CO_2 photocatalytic reduction, representing a vital solar fuel utilized in various applications such as electricity production through steam-generated machines and gas turbines. Kamal and colleagues used TiO_2 decorated N-rGO with Au nanoparticles to achieve selective production of CH_4 at an impressive rate of approximately 742.39 μmol g^{-1} h^{-1} under visible irradiation for 4 h in a gas-phase batch reactor.[92] The composite demonstrated a remarkable 60-fold increase in electron consumption, significantly enhancing CH_4 production, as verified through gas chromatography equipped with flame ionization and thermal conductivity detectors. Density functional theory analysis of the product distribution during CO_2 photocatalytic reduction revealed a significant role played by positive spin density with nitrogen and carbon, contingent upon the utilization of pyridinic-N, pyrrolic-N, and negative spin basal plane of carbon. Mapping the spin density of N-rGO unveiled the formation of the carboxylic radical (*COOH) as a reactive intermediate during the initial electron–proton transfer in the CO_2 photocatalytic reduction process, leading to CH_4 formation. The stabilization of *COOH depends on the specific reaction pathway during its subsequent reduction to solar fuels, as depicted in Fig. 8b for CH_4 formation.[92] In another study, an impressive CH_4 production rate (953.72 μmol g^{-1}) was achieved using a nanocomposite of indium oxide (In_2O_3) with rGO.[88] This nanocomposite outperformed pure In_2O_3 in CH_4 production, which can be attributed to prolonged charge carrier separation duration and enhanced charge transfer from In_2O_3 to rGO under visible light irradiation. The oxidation of H_2O was found to generate H_2 ions (H^+), which, when combined with photogenerated electrons, facilitated the formation of CH_4 and C_2H_5OH. A reduced recombination rate and a shift in energy bandgap contributed to the increased yield of CH_4 as a primary product. Additionally, rGO significantly enhanced O vacancy defects and altered bandgaps, creating active sites for CO_2 adsorption and thereby boosting CH_4 production.[88,125] These findings offer valuable insights into various strategies for achieving efficient photocatalytic reduction of CO_2 into CH_4.

4.2. Alcohol production

CH_3OH and C_2H_5OH have been identified as key alcohol products in the selective photocatalytic reduction of CO_2. Interestingly, it was observed that conducting CO_2 photocatalytic reduction in aqueous media often results in higher production rate of CH_3OH compared to other products, as outlined in Table 1.[123] The reaction can be triggered either by a conduction band electron of the photocatalyst reducing CO_2 directly or by the dissociated form of CO_2 in water, leading to the formation of carbonic acid, bicarbonate or carbonate ions, depending on the pH conditions. In aqueous media, CO_2 predominantly exists as carbonic acid/CO_2 at pH < 4, as carbonate ions at pH > 10, and as a mixture of all three forms at pH 7. Possible pathways for the production of CH_3OH during the photocatalytic reduction of CO_2 in aqueous media are illustrated in Fig. 8c.[123] Given its direct usability as a fuel, CH_3OH offers advantages, especially when applied in liquid systems. Studies, including those by Shih and coworkers highlight CH_3OH and C_2H_5OH as ideal fuels in terms of storage and transportation, given their liquid state compared to other alternatives.[126] Additionally, H_2 evolution often competes during alcohol production, but its separation is feasible since H_2 is obtained in the gas phase while alcohol remains in liquid form.[126]

A group of researchers adopted a simple thermal copolymerization technique to synthesize g-C_3N_4 with a lowered bandgap, which was further combined with rGO for CH_3OH production, achieving an impressive yield of 114 μmol g^{-1} h^{-1}. The CH_3OH yield notably improved as the rGO content increased from 0 to 5 wt%, resulting in a quantum yield of 0.63%. The composite denoted as G_5A_5/rGO_5 showed 83% higher selectivity for CH_3OH in 6 cycles, attributed to the increased charge carrier separation.[41] The 2D/2D heterojunction formed between rGO and g-C_3N_4 increases charge transport, lowers recombination of charge carriers, and extends the electron lifetime for reduction reactions.[41] In another study, a composite of GO and TiO_2 was prepared using the liquid-phase deposition method for the production of CH_3OH (47 μmol g^{-1} h^{-1}, at pH 4) and C_2H_5OH (144.7 μmol g^{-1} h^{-1}, at pH 11) under UV-visible irradiation. To mitigate the issue of H_2

formation during photocatalytic reduction of CO_2 with water, copper was used as a co-catalyst to trap more electrons in the conduction band.[79] The effect of both copper(I)oxide and pH was considered during the photocatalytic reaction for alcohol production. The pH of the solution affects the solubility of CO_2 in water, thus affecting carbonate ion production and protonation equilibrium. Furthermore, it was found that proton concentration is higher at lower pH, potentially reducing CO_2 reduction potential with negative species protonation involving electron transfer to CO_2.[127] The carbonate ion accepts the electron from co-catalyst copper(I)oxide to form a CO_2 radical ($^{\bullet}CO_2$), which then reacts with a H_2 radical ($^{\bullet}H$) to form a methoxyl radical. Under acidic conditions (pH 4), methoxyl radicals undergo protonation to form CH_3OH, while under alkaline conditions (pH 11), C_2H_5OH is produced through a radical substrate reaction. Additionally, higher adsorption capacity of the photocatalyst and the movement of electrons between the two phases create synergistic interactions that augment the efficiency of the photocatalytic reduction reaction.[79] Research has revealed that during CO_2 photocatalytic reduction, H_2 and carbon atoms can be attached, leading to the cleavage of C–O bonds and the transformation of $^{\bullet}CO_2$ into CO over the catalyst surface. The presence of a co-catalyst bond plays a crucial role in CH_3OH formation. If the bond is weak, the final product will be CO, and if the bond is relatively strong, the carbon radical attaches with four $^{\bullet}H$, leading to CH_3OH formation.[128] For the analysis of alcohol produced in the liquid phase, a gas chromatograph equipped with a flame ionization detector and helium as a carrier gas can be employed, while for qualitative analysis, nuclear magnetic resonance or gas chromatography-mass spectrometry techniques are suitable.[90,120]

4.3. Carboxylic acid production

Carboxylic acids, specifically HCOOH and acetic acid, are among the prominent products generated in CO_2 photocatalytic reduction.[76,129] A suitable photocatalyst, utilizing GO modified cobalt metallated aminoporphyrin (GO-Co-ATTP), was developed for the photocatalytic reduction of CO_2 into HCOOH, achieving a yield of almost 96.49 μmol for 2 h under visible light irradiation.[84] The GO-Co-ATPP material is a nanohybrid composed of GO covalently bonded with porphyrin, designed to facilitate charge-transfer processes. In this system, graphene serves as the electron donor, while porphyrin functions as the electron acceptor. As depicted in Fig. 9, the enzymatic conversion of CO_2 to HCOOH by formate dehydrogenase is driven by the regenerated nicotinamide adenine dinucleotide (NADH). During the cyclic process, NAD^+ released from the enzyme participates in the photoregeneration of NADH, which is subsequently reused for the reduction of CO_2 to HCOOH.[84] At times, the formation of HCOOH may initiate with hydrogenation, where a H atom combines with one O atom of $^{\bullet}CO_2$ to form a carboxyl radical. In a highly polar aqueous environment, the carboxyl radical may react with $^{\bullet}H$ to form HCOOH.[128] Alternative pathways for carboxylic acid production may involve some anion radicals, aqueous electrons in solvated form, and other derivatives of $CO_2^{\bullet-}$.[130] Another anticipated outcome of CO_2 photocatalytic reduction is oxalic acid, resulting from one electron photocatalytic reduction of $CO_2^{\bullet-}$ to the oxalate anion.[119] After photocatalytic reduction of CO_2, carboxylic acid obtained in the liquid phase can be analyzed by high-performance liquid chromatography.[120]

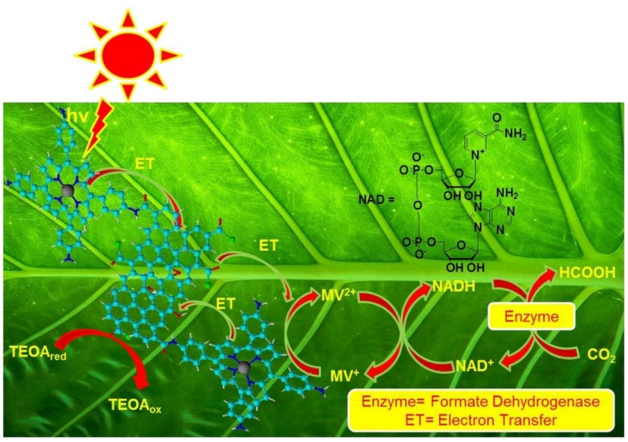

Fig. 9 Plausible pathway for the conversion of CO_2 into formic acid over graphene oxide modified cobalt metallated aminoporphyrin. Reproduced with permission from ref. 67, copyright 2018, Elsevier Ltd.

4.4. Aldehyde production

Aldehydes, including CH_3CHO and HCHO, are potential products of CO_2 photocatalytic reduction. These compounds can be detected through gas chromatography, with quantification achieved using a flame ionization detector equipped column or Nash's colorimetry. High-performance liquid chromatography can be used to determine the concentration of aldehydes in the liquid phase after derivatization, as aldehydes are typically obtained at much lower concentrations.[90,120] Shown and coworkers successfully obtained CH_3CHO and CH_3OH through the photocatalytic reduction of CO_2 using a composite of copper nanoparticles (5–10 wt%) decorated over GO, synthesized *via* a one-pot microwave method. Under optimum conditions with 2 h of irradiation, the reported yields of CH_3CHO and CH_3OH were 3.88 μmol g_{cat}^{-1} h^{-1} and 2.94 μmol g_{cat}^{-1} h^{-1}, respectively.[77] In this scenario, the activation of CO_2 occurs as electrons transfer from the d-orbitals of the metal to the π* orbital of the C–O bond, followed by multielectron reduction, resulting in the production of CH_3CHO and CH_3OH as products.[77] In a recent study, a nanocomposite of p-type nickel oxide decorated over n-type ceric oxide/rGO produced nearly 4 times more HCHO than pure ceric oxide (CeO_2).[89] The study revealed that the p–n junction formed between nickel oxide and CeO_2 modified the bandgap energy resulting in a red-shift in the nanocomposite. This heterojunction facilitated an increased generation of charge carriers, with the metallic properties of nickel enabling enhanced photon absorption. Additionally, oxygen vacancies in the nanocomposite, induced by CeO_2 and evidenced by an increased Ce–O bond length, played a critical role in capturing CO_2 molecules. CO_2 is transformed into $^{\bullet}CO_2$ after absorption, which lowers the activation energy and

increases the reduction rate.[89] Few studies in the literature have reported the conversion of alcohols into their corresponding aldehydes to meet specific demands in industries such as pharmaceutical, fragrance, and confectionery. For instance, Yang and Xu synthesized a composite from exfoliated GO and TiO_2 that was employed under visible light to successfully produce benzaldehyde from benzyl alcohol.[131]

The exploration of graphene-based composites in the production of value-added chemicals/fuels opens up new possibilities for efficient and sustainable catalytic processes, contributing to advancements in the synthesis of valuable chemical intermediates and fine chemicals. Continued research and optimization of these composite catalysts are essential to fully harness their potential and enable their practical implementation in the industrial sector.

5. Challenges and future prospects in CO_2 photocatalytic reduction

CO_2 photocatalytic reduction is a promising technology, but it faces several challenges, particularly related to the inert nature of CO_2, a stable and unreactive molecule. Some of the key challenges include:

(a) High activation energy: The conversion of CO_2 into useful products necessitates overcoming a significant activation energy barrier. CO_2 is a thermodynamically stable molecule making it challenging to initiate and drive the reaction using solar energy alone.[132] Consequently, the photocatalytic reduction process often demands the use of catalysts to lower the activation energy.

(b) Low reaction rates: The kinetic inertness of CO_2 renders its reduction to fuels *via* photocatalytic processes a slow and inefficient endeavor. Enhancing the reaction rates to improve the overall process efficiency remains a major challenge.

(c) Surface reaction kinetics: The kinetics of surface reactions, including adsorption and desorption of CO_2 and reaction intermediates, can significantly impact the overall efficiency of the photocatalytic process. Understanding and optimizing these kinetics are essential.

(d) Selectivity and product separation: CO_2 photocatalytic reduction can yield multiple products depending on the photocatalyst and reaction conditions. Efficient separation and extraction of the desired products from the reaction mixture can be challenging, especially when multiple products are formed. Thus, developing effective separation techniques is crucial for the practical implementation of this technology.[133] Furthermore, there is currently no well-defined framework for tailoring photocatalysts to selectively drive the reduction process toward the formation of a single product. Additionally, in scenarios involving product distribution, computational studies exploring the reaction pathways and the factors influencing the generation of specific products are essential. Such studies could guide the design and modification of photocatalysts and elucidate the structural characteristics of active sites that promote the production of selective products.

(e) Understanding the reaction mechanism: Gaining a detailed understanding of the intricate reaction mechanisms underlying CO_2 photocatalytic reduction is vital. Elucidating the various pathways and intermediates formed during the process is essential for targeted catalyst design and optimization.

(f) Photocatalyst development: The efficiency and selectivity of CO_2 photocatalytic reduction are strongly influenced by the choice and design of photocatalysts. Developing efficient and stable photocatalysts that can not only perform under solar illumination but also withstand prolonged use is an ongoing challenge.

(g) Photocatalyst bandgap and stability: The ideal photocatalyst should have a bandgap that efficiently absorbs solar energy and promotes electron transfer to CO_2. However, many photocatalysts suffer from degradation and reduced efficiency due to photocorrosion and stability issues.

(h) Mass transport limitations: Since CO_2 is typically supplied as a gas, its availability at the catalytic sites is constrained by both its diffusion rate and solubility in the reaction medium.

(i) Photon absorption efficiency: To drive the photocatalytic reduction reaction, the photocatalyst must efficiently absorb solar photons. Enhancing light-harvesting capabilities and optimizing the photocatalyst design to utilize a broader visible light spectrum is an active area of research.

(j) Integrating with existing infrastructure: Integrating CO_2 photocatalytic reduction technologies into existing industrial and energy infrastructure poses challenges. Thus, several factors, including compatibility, scalability, and ease of integration, need careful consideration.

(k) Real-world conditions: CO_2 photocatalytic reduction must proceed effectively under varying real-world conditions, including changes in sunlight intensity, temperature, and humidity. Therefore, developing robust systems capable of withstanding environmental fluctuations is essential.

(l) Economic viability: Assessing and improving the economic viability of CO_2 photocatalytic reduction processes is crucial for widespread adoption. Evaluating the costs associated with materials, catalysts, and energy input *versus* the benefits of fuel production is an enduring concern.

(m) Scale-up and cost: While promising at the lab scale, scaling up CO_2 photocatalytic reduction processes for practical applications poses challenges. Additionally, evaluating the cost-effectiveness of these processes is crucial for commercial viability.

Addressing these challenges requires interdisciplinary research efforts in materials science, catalysis, photochemistry, and chemical engineering. Ongoing research and development are essential to optimize CO_2 photocatalytic reduction technology, making it a viable and scalable option for sustainable CO_2 reduction.

6. Challenges specific to graphene-derived photocatalysts and scalability of the CO_2 photoreduction system

Although graphene-based materials have gained significant attention as photocatalysts for CO_2 reduction, their long-term

stability and performance are often hindered by several challenges. Specifically, GO-based photocatalysts suffer from photochemical and thermal deoxygenation of surface functional groups, including epoxy, hydroxyl, and carboxyl moieties, which disrupt the π-conjugated network and degrade conductivity under prolonged illumination.[134,135] Variations in GO synthesis (*e.g.*, classical *versus* modified Hummers' methods) result in materials with widely differing C/O ratios, defect densities, and lateral flake sizes, leading to pronounced batch-to-batch inconsistencies in activity.[136,137] Furthermore, residual oxidants and carbonaceous byproducts from chemical reduction can foul active sites or leach into reaction streams, undermining both conversion efficiency and product selectivity.[138] To overcome these issues, "green" reduction using L-ascorbic acid provides rGO with tunable oxygen content and minimal impurities.[139] Furthermore, heteroatom doping, particularly N-doping in TiO_2/rGO hybrids, reinforces the graphene lattice, anchors CO_2 intermediates, and preserves more than 85% of initial activity over 35 h of continuous photoreduction.[140,141] Moreover, careful control of nitrogen content and bonding configurations further stabilizes functional groups and supports long-term durability.[140] These sustainable strategies collectively ensure reproducible and durable performance of graphene-derived photocatalysts under extended solar-driven operation.

In parallel with addressing these material-specific challenges, scalability remains a critical hurdle in advancing CO_2 photoreduction technologies toward practical application. Recent prototype demonstrations offer promising solutions at both the meso and pilot scales. A meso-scale continuous-flow photochemical reactor employing immobilized Pt/TiO_2/rGO films achieved enhanced CO_2 conversion rates by optimizing flow dynamics and light distribution over 12 h of operation.[142] At a larger scale, a continuous-flow reactor system managing triple-phase interfaces *via* gas and liquid flow exhibited 10- to 24-fold increases in CO production rates compared to batch reactors, with a CO selectivity of 93.2% and long-term stability exceeding 780 min.[143] These case studies underscore the importance of reactor design for uniform illumination, mass transfer, and catalyst immobilization in scaling up CO_2 photoreduction technologies. Although most studies remain at the bench scale, recent prototype systems demonstrate practical feasibility. For instance, a mini-pilot photoreactor combining H_2O splitting, H_2 separation, and CO_2 methanation operated outdoors under natural sunlight for three days, producing sufficient crude methane to power a Stirling engine.[144] Reactor designs leveraging compound-parabolic collectors, panel reactors, and continuous-flow schemes, coupled with catalyst immobilization and optimized light management, are now being explored for pilot-scale deployment. These developments highlight a clear pathway from material innovation to real-world solar fuel production systems.

7. Conclusion

This review underscores the promising prospects of CO_2 photocatalytic reduction for generating solar fuels and value-added chemicals, particularly through the use of graphene-based photocatalysts. Despite the progress in developing numerous photocatalysts over the years, the challenge of designing an efficient CO_2 photoreduction system persists. The integration of graphene with appropriate semiconductors brings about a significant improvement in various physicochemical properties, including improved charge separation, enhanced electron transport, strong adsorption capabilities, and augmented photocatalytic performance. This synergistic effect ultimately enhances the overall performance of the composite materials.

Nevertheless, graphene encounters inherent challenges that require fundamental and theoretical solutions. Approaches such as defect-induced modification and advanced doping methods can significantly enhance the properties of graphene-based composites. Since graphene acts as an electron acceptor and reduces recombination, detailed analyses such as photocurrent response and electron conductivity measurements are crucial for understanding and optimizing the charge carrier dynamics of graphene-based photocatalysts during CO_2 photocatalytic reduction. Moreover, a comprehensive understanding of the mechanisms leading to the formation of various products during CO_2 photocatalytic reduction is essential. This understanding can contribute to the further development of mechanisms that enhance product selectivity, ensuring that the carbon source in the products is derived from CO_2 rather than graphene. The potential occurrence of the H_2 evolution reaction, particularly during alcohol production, introduces an additional challenge that requires careful consideration. Furthermore, the stability of the composite against photocorrosion is a critical aspect that needs attention during CO_2 photocatalytic reduction reactions. On the other hand, the accountability of graphene composites is substantial due to their diverse properties and unique structure. Therefore, overcoming challenges related to oxidation sites and defects in graphene to produce high-quality composites remains a formidable task. Additionally, the storage of solar fuels produced through CO_2 photoreduction presents significant challenges that hinder the scalability and practicality of this technology. Considering the multiscale challenges, it seems particularly interesting to fortify the overall process efficiency and key material properties to achieve high conversion yields of CO_2 to renewable fuels.

Data availability

Data will be made available upon request.

Conflicts of interest

There are no conflicts to declare.

Acknowledgements

This work was financially supported by the Department of Science and Technology (DST), Government of India, through its Solar Energy Research and Development (SERD) initiative (File No. DST/TMD/CERI/RES/2020/41). Manisha Sain

acknowledges the financial support provided by the Indian Institute of Technology Kharagpur, West Bengal, India, for her doctoral study. Debanjali Dey is thankful for the financial support provided by the Ministry of Education, Government of India, through its Prime Minister's Research Fellowship scheme for her doctoral study.

References

1 S. Chowdhury and R. Balasubramanian, *J. CO_2 Util.*, 2016, **13**, 50–60.
2 S. Chowdhury and R. Balasubramanian, *Sci. Rep.*, 2016, **6**, 21537.
3 R. L. Singh and P. K. Singh, in *Principles and Applications of Environmental Biotechnology for a Sustainable Future*, Springer, Singapore, 2017, pp. 13–41.
4 K. Li, X. An, K. H. Park, M. Khraisheh and J. Tang, *Catal. Today*, 2014, **224**, 3–12.
5 D. S. A. Simakov, Photocatalytic Reduction of CO_2, in *Renewable synthetic fuels and chemicals from carbon dioxide: Fundamentals, catalysis, design considerations and technological challenges*, Springer, Cham, Switzerland, 2017, pp. 43–54.
6 S. Nagireddi, J. R. Agarwal and D. Vedapuri, *ACS Eng. Au*, 2024, **4**, 22–48.
7 V. Khare, S. Nema and P. Baredar, *Renew. Sustain. Energy Rev.*, 2016, **58**, 23–33.
8 K. K. Jaiswal, C. R. Chowdhury, D. Yadav, R. Verma, S. Dutta, K. S. Jaiswal, B. Sangmesh and K. S. K. Karuppasamy, *Energy Nexus*, 2022, **7**, 100118.
9 D. Zhang and J. Song, *Procedia IUTAM*, 2014, **10**, 319–327.
10 W. M. Budzianowski, *Int. J. Glob. Warm.*, 2017, **12**, 272.
11 J. Godin, W. Liu, S. Ren and C. C. Xu, *J. Environ. Chem. Eng.*, 2021, **9**, 105644.
12 P. Ganji, R. K. Chowdari and B. Likozar, *Energy Fuels*, 2023, **37**, 7577–7602.
13 M. Bonchio, J. Bonin, O. Ishitani, T.-B. Lu, T. Morikawa, A. J. Morris, E. Reisner, D. Sarkar, F. M. Toma and M. Robert, *Nat. Catal.*, 2023, **6**, 657–665.
14 Y. Huang, C.-F. Yan, C.-Q. Guo and S.-L. Huang, *Int. J. Photoenergy*, 2015, **2015**, 1–11.
15 R. Xu, *AIP Conf. Proc.*, 2024, **3144**, 020004.
16 D. Gust, T. A. Moore and A. L. Moore, *Acc. Chem. Res.*, 2009, **42**, 1890–1898.
17 A. Kudo and Y. Miseki, *Chem. Soc. Rev.*, 2009, **38**, 253–278.
18 D. Kim, K. K. Sakimoto, D. Hong and P. Yang, *Angew. Chem., Int. Ed.*, 2015, **54**, 3259–3266.
19 M. G. Kibria and Z. Mi, *J. Mater. Chem. A*, 2016, **4**, 2801–2820.
20 S. Patial, R. Kumar, P. Raizada, P. Singh, Q. Van Le, E. Lichtfouse, D. Le Tri Nguyen and V. H. Nguyen, *Environ. Res.*, 2021, **197**, 111134.
21 M. Lashgari, S. Soodi and P. Zeinalkhani, *J. CO_2 Util.*, 2017, **18**, 89–97.
22 D. Zhang, Y. Wang, Y. Wang, Y. Zhang and X. M. Song, *J. Alloys Compd.*, 2020, **815**, 152377.
23 Y. Shen, Q. Han, J. Hu, W. Gao, L. Wang, L. Yang, C. Gao, Q. Shen, C. Wu, X. Wang, X. Zhou, Y. Zhou and Z. Zou, *ACS Appl. Energy Mater.*, 2020, **3**, 6561–6572.
24 H. Huang, K. Liu, K. Chen, Y. Zhang, Y. Zhang and S. Wang, *J. Phys. Chem. C*, 2014, **118**, 14379–14387.
25 G. Zhang, J. Zhang, M. Zhang and X. Wang, *J. Mater. Chem.*, 2012, **22**, 8083–8091.
26 W. J. Ong, L. L. Tan, S. P. Chai and S. T. Yong, *Chem. Commun.*, 2015, **51**, 858–861.
27 N. Shehzad, M. Tahir, K. Johari, T. Murugesan and M. Hussain, *J. Environ. Chem. Eng.*, 2018, **6**, 6947–6957.
28 H. Y. Hafeez, S. K. Lakhera, N. Narayanan, S. Harish, Y. Hayakawa, B. K. Lee and B. Neppolian, *ACS Omega*, 2019, **4**, 880–891.
29 A. Razzaq, A. Sinhamahapatra, T. H. Kang, C. A. Grimes, J. S. Yu and S. Il, *Appl. Catal., B*, 2017, **215**, 28–35.
30 L. Cheng, Q. Xiang, Y. Liao and H. Zhang, *Energy Environ. Sci.*, 2018, **11**, 1362–1391.
31 K. Chu, X. hu Wang, Y. biao Li, D. jian Huang, Z. rong Geng, X. long Zhao, H. Liu and H. Zhang, *Mater. Des.*, 2018, **140**, 85–94.
32 G. G. Naumis, S. Barraza-Lopez, M. Oliva-Leyva and H. Terrones, *Rep. Prog. Phys.*, 2017, **80**, 096501.
33 K. S. Novoselov, A. K. Geim, S. V. Morozov, D. Jiang, Y. Zhang, S. V. Dubonos, I. V. Grigorieva and A. A. Firsov, *Science*, 2004, **306**, 666–669.
34 D. G. Papageorgiou, I. A. Kinloch and R. J. Young, *Prog. Mater. Sci.*, 2017, **90**, 75–127.
35 J. Low, J. Yu and W. Ho, *J. Phys. Chem. Lett.*, 2015, **6**, 4244–4251.
36 R. Zhang, Z. Huang, C. Li, Y. Zuo and Y. Zhou, *Appl. Surf. Sci.*, 2019, **475**, 953–960.
37 M. Y. Akram, T. Ashraf, M. S. Jagirani, A. Nazir, M. Saqib and M. Imran, *Catalysts*, 2024, **14**, 343.
38 Y. Liu, J. Shang and T. Zhu, *J. Mater. Chem. C*, 2024, **12**, 9293–9304.
39 Y. Liu, Y. Wang, J. Shang, J. Peng and T. Zhu, *Appl. Catal. B Environ. Energy*, 2024, **350**, 123937.
40 D. Liu, Y. Hu, R. Chen, S. Guo, Y. Yang and X. Wang, *Catal. Sci. Technol.*, 2025, **15**, 427–434.
41 R. C. Sahoo, H. Lu, D. Garg, Z. Yin and H. S. S. R. Matte, *Carbon*, 2022, **192**, 101–108.
42 Y. Zhang, L. Zheng, J. Jia, K. Li, T. Zhang and H. Yu, *Colloids Surf. A Physicochem. Eng. Asp.*, 2022, **639**, 128321.
43 P. J. J. Sagayaraj, A. Augustin, M. Shanmugam, B. Honnappa, T. S. Natarajan, K. Wilson, A. F. Lee and K. Sekar, *Energy Technol.*, 2023, **11**, 2300563.
44 M. Q. Yang and Y. J. Xu, *Nanoscale Horiz.*, 2016, **1**, 185–200.
45 V. P. Indrakanti, J. D. Kubicki and H. H. Schobert, *Energy Environ. Sci.*, 2009, **2**, 745.
46 X. Chang, T. Wang and J. Gong, *Energy Environ. Sci.*, 2016, **9**, 2177–2196.
47 W. Tu, Y. Zhou and Z. Zou, *Adv. Mater.*, 2014, **26**, 4607–4626.
48 H. Shi, G. Chen, C. Zhang and Z. Zou, *ACS Catal.*, 2014, **4**, 3637–3643.
49 M. Alhaddad and A. Shawky, *Ceram. Int.*, 2021, **47**, 9763–9770.

50 J. Jin and T. He, *Appl. Surf. Sci.*, 2017, **394**, 364–370.
51 D. A. Reddy, E. H. Kim, M. Gopannagari, R. Ma, P. Bhavani, D. P. Kumar and T. K. Kim, *ACS Sustain. Chem. Eng.*, 2018, **6**, 12835–12844.
52 U. J. Etim, C. Zhang and Z. Zhong, *Nanomaterials*, 2021, **11**, 3265.
53 M. Nolan and M. Fronzi, *Catal. Today*, 2019, **326**, 68–74.
54 K. M. Megha, A. Banerjee and T. K. Ghanty, *Phys. Chem. Chem. Phys.*, 2020, **22**, 16877–16886.
55 J. M. Weber, *Int. Rev. Phys. Chem.*, 2014, **33**, 489–519.
56 J. Lee, D. C. Sorescu and X. Deng, *J. Am. Chem. Soc.*, 2011, **133**, 10066–10069.
57 C. Wang, X. Zhang and Y. Liu, *Appl. Surf. Sci.*, 2015, **358**, 28–45.
58 X. Li, J. Wen, J. Low, Y. Fang and J. Yu, *Sci. China Mater.*, 2014, **57**, 70–100.
59 C. Hiragond, S. Ali, S. Sorcar and S. In, *Catalysts*, 2019, **9**, 370.
60 S. Lu, F. Lou and Z. Yu, *Catalysts*, 2022, **12**, 228.
61 X. Jiao, K. Zheng, Z. Hu, Y. Sun and Y. Xie, *ACS Cent. Sci.*, 2020, **6**, 653–660.
62 M. Isah, R. Lawal and S. A. Onaizi, *Green Chem. Eng.*, 2025, **6**, 305–334.
63 R. S. Ruoff, *Carbon*, 2018, **132**, 802.
64 S. Xing, Y. Liu, X. Liu, M. Li, J. Fu, P. Liu, P. Lv and Z. Wang, *Appl. Catal., B*, 2020, **269**, 118718.
65 A. Atmanlı, B. Yüksel, E. İleri and A. Deniz Karaoglan, *Energy Convers. Manag.*, 2015, **90**, 383–394.
66 W. Cao, W. Wang, H. Shi, J. Wang, M. Cao, Y. Liang and M. Zhu, *Nano Res.*, 2018, **11**, 1437–1446.
67 L. G. Devi and R. Kavitha, *Appl. Catal., B*, 2013, **140–141**, 559–587.
68 V. Saxena and D. K. Aswal, *Semicond. Sci. Technol.*, 2015, **30**, 064005.
69 S. G. Kumar and K. S. R. K. Rao, *Appl. Surf. Sci.*, 2017, **391**, 124–148.
70 W. Fan, Q. Zhang and Y. Wang, *Phys. Chem. Chem. Phys.*, 2013, **15**, 2632–2649.
71 J. Li, L. Niu, Z. Zheng and F. Yan, *Adv. Mater.*, 2014, **26**, 5239–5273.
72 J. M. Barrera-Andrade, E. Albiter, M. A. Valenzuela and E. Rojas García, Graphene-Based Photocatalysts for CO_2 Reduction, in *Graphene-Based Photocatalysts, Adv. Struct. Mater.*, ed. M. R. Johan, M. N. Naseer, M. Ikram, A. A. Zaidi and Y. Abdul Wahab, Springer, Cham, Switzerland, 2024, vol. 217, pp. 709–729.
73 M. Khan, M. Khan, M. Khan, H. Javaid and S. Musaddiq, Harnessing the Power of Graphene: A Critical Analysis of Graphene-Based Photocatalysts for CO_2 Reduction, in *Graphene-Based Photocatalysts for Hydrogen Production and Environmental Remediation, Adv. Struct. Mater.*, ed. M. N. Naseer, M. Ikram, A. A. Zaidi, Y. Abdul Wahab and M. R. Johan, Springer, Cham, Switzerland, 2024, vol. 219, pp. 427–448.
74 H. Hsu, I. Shown, H. Wei, Y. Chang, H. Du, Y. Lin, C. Tseng, C. Wang, L. Chen, Y. Lin and K. Chen, *Nanoscale*, 2013, **5**, 262–268.
75 P.-Q. Wang, Y. Bai, P.-Y. Luo and J.-Y. Liu, *Catal. Commun.*, 2013, **38**, 82–85.
76 J. Cheng, M. Zhang, G. Wu, X. Wang, J. Zhou and K. Cen, *Environ. Sci. Technol.*, 2014, **48**, 7076–7084.
77 I. Shown, H. C. Hsu, Y. C. Chang, C. H. Lin, P. K. Roy, A. Ganguly, C. H. Wang, J. K. Chang, C. I. Wu, L. C. Chen and K. H. Chen, *Nano Lett.*, 2014, **14**, 6097–6103.
78 L. L. Tan, W. J. Ong, S. P. Chai and A. R. Mohamed, *Appl. Catal., B*, 2015, **166–167**, 251–259.
79 L. M. Pastrana-Martínez, A. M. T. Silva, N. N. C. Fonseca, J. R. Vaz, J. L. Figueiredo and J. L. Faria, *Top. Catal.*, 2016, **59**, 1279–1291.
80 R. Gusain, P. Kumar, O. P. Sharma, S. L. Jain and O. P. Khatri, *Appl. Catal., B*, 2016, **181**, 352–362.
81 Z. Xiong, Y. Luo, Y. Zhao, J. Zhang, C. Zheng and J. C. S. Wu, *Phys. Chem. Chem. Phys.*, 2016, **18**, 13186–13195.
82 Q. Zhang, L. Huang, S. Kang, C. Yin, Z. Ma, L. Cui and Y. Wang, *RSC Adv.*, 2017, **7**, 43642–43647.
83 L. L. Tan, W. J. Ong, S. P. Chai and A. R. Mohamed, *Chem. Eng. J.*, 2017, **308**, 248–255.
84 S. Kumar, R. K. Yadav, K. Ram, A. Aguiar, J. Koh and A. J. F. N. Sobral, *J. CO_2 Util.*, 2018, **27**, 107–114.
85 S. Sorcar, J. Thompson, Y. Hwang, Y. H. Park, T. Majima, C. A. Grimes, J. R. Durrant and S. Il, *Energy Environ. Sci.*, 2018, **11**, 3183–3193.
86 X. Wang, Q. Li, C. Zhou, Z. Cao and R. Zhang, *J. Colloid Interface Sci.*, 2019, **554**, 335–343.
87 T. Wu, C. Zhu, D. Han, Z. Kang and L. Niu, *Nanoscale*, 2019, **11**, 22980–22988.
88 P. Devi and J. P. Singh, *J. CO_2 Util.*, 2021, **43**, 101376.
89 H. R. Park, A. U. Pawar, U. Pal, T. Zhang and Y. S. Kang, *Nano Energy*, 2021, **79**, 105483.
90 H. T. Lien, Y. C. Chang, C. Y. Huang, H. C. Hsu, S. T. Chang, D. P. Wong, C. H. Wang, C. H. Wang, K. H. Chen and L. C. Chen, *J. Chem. Phys.*, 2021, **154**, 164707.
91 N. Nandal, P. K. Prajapati, B. M. Abraham and S. L. Jain, *Electrochim. Acta*, 2022, **404**, 139612.
92 K. M. Kamal, R. Narayan, N. Chandran, S. Popović, M. A. Nazrulla, J. Kovač, N. Vrtovec, M. Bele, N. Hodnik, M. M. Kržmanc and B. Likozar, *Appl. Catal., B*, 2022, **307**, 121181.
93 A. Hasani, M. A. Teklagne, H. H. Do, S. H. Hong, Q. Van Le, S. H. Ahn and S. Y. Kim, *Carbon Energy*, 2020, **2**, 158–175.
94 G. Žerjav, M. S. Arshad, P. Djinović, I. Junkar, J. Kovač, J. Zavašnik and A. Pintar, *Nanoscale*, 2017, **9**, 4578–4592.
95 P. Huo, X. Shi, W. Zhang, P. Kumar and B. Liu, *J. Mater. Sci.*, 2021, **56**, 6031–6051.
96 L. Y. Lin, Y. Nie, S. Kavadiya, T. Soundappan and P. Biswas, *Chem. Eng. J.*, 2017, **316**, 449–460.
97 V. Deerattrakul, P. Dittanet, M. Sawangphruk and P. Kongkachuichay, *J. CO_2 Util.*, 2016, **16**, 104–113.
98 H. Jung, H. Choi, Y. Song, J. H. Kim and Y. Yoon, *Nanoscale Adv.*, 2024, **6**, 4611–4624.
99 Y. Li, M. Zhou, B. Cheng and Y. Shao, *J. Mater. Sci. Technol.*, 2020, **56**, 1–17.
100 Z. Otgonbayar, Y. Liu and W. Oh, *J. Environ. Chem. Eng.*, 2023, **11**, 109884.

101 S. Yin, J. Li, L. Sun, X. Li, D. Shen, X. Song, P. Huo, H. Wang and Y. Yan, *Inorg. Chem.*, 2019, **58**, 15590–15601.
102 Y. Ding, Y. Zhou, W. Nie and P. Chen, *Appl. Surf. Sci.*, 2015, **357**, 1606–1612.
103 L. Zhu, Y. Wang, C. Qin and J. Cao, *J. Phys. Chem. C*, 2022, **126**, 16702–16709.
104 J. Yu, J. Jin, B. Cheng and M. Jaroniec, *J. Mater. Chem. A*, 2014, **2**, 3407.
105 H. Jung, K. M. Cho, K. H. Kim, H.-W. Yoo, A. Al-Saggaf, I. Gereige and H. Jung, *J. Mater. Chem. A*, 2018, **6**, 5718–5724.
106 T. Van Khai, L. N. Long, M. T. Phong, P. T. Kien, L. Van Thang and T. D. Lam, *J. Electron. Mater.*, 2020, **49**, 969–979.
107 C. Das, T. Shafi, S. Pan, Mu. Naushad, B. K. Dubey and S. Chowdhury, *ACS Appl. Nano Mater.*, 2023, **6**, 12991–13000.
108 Z. Du, H. Cai, Z. Zhao, Z. Guo, J. Lin, Y. Huang, C. Tang, G. Chen and Y. Fang, *Sep. Purif. Technol.*, 2023, **311**, 123321.
109 R. Manna, G. Bhattacharya, S. Raj and A. N. Samanta, *J. Environ. Chem. Eng.*, 2024, **12**, 111722.
110 N. Kumar, S. Kumar, R. Gusain, N. Manyala, S. Eslava and S. S. Ray, *ACS Appl. Energy Mater.*, 2020, **3**, 9897–9909.
111 L. Velasco Davoise, R. Peña Capilla and A. M. Díez-Pascual, *Polymers*, 2022, **14**, 1828.
112 X. Liu, X. Zhao, J. Yan, Y. Huang, T. Li and P. Liu, *Carbon*, 2021, **178**, 273–284.
113 A. Sheelam, A. Muneeb, B. Talukdar, R. Ravindranath, S. Huang, C. Kuo and R. Sankar, *J. Appl. Electrochem.*, 2020, **50**, 979–991.
114 R. Castro-Muñoz, J. Buera-González, Ó. de la Iglesia, F. Galiano, V. Fíla, M. Malankowska, C. Rubio, A. Figoli, C. Téllez and J. Coronas, *J. Membr. Sci.*, 2019, **582**, 423–434.
115 J. Liu, Y.-H. Zhang, Z.-M. Bai, Z.-A. Huang and Y.-K. Gao, *Chin. Phys. B*, 2019, **28**, 048101.
116 L. Zhou, H. Kamyab, A. Surendar, A. Maseleno, A. Z. Ibatova, S. Chelliapan, N. Karachi and Z. Parsaee, *J. Photochem. Photobiol. A*, 2019, **368**, 30–40.
117 A. Ali and W.-C. Oh, *Sci. Rep.*, 2017, **7**, 1867.
118 R. Wang, L. Du, Y. Liu, Y. Gu, X. Li and Y. Li, *2D Mater.*, 2024, **11**, 015014.
119 M. R. Hoffmann, J. A. Moss and M. M. Baum, *Dalton Trans.*, 2011, **40**, 5151–5158.
120 J. Hong, W. Zhang, J. Ren and R. Xu, *Anal. Methods*, 2013, **5**, 1086–1097.
121 D. Liu, Y. Hu, R. Chen, S. Guo, Y. Yang and X. Wang, *Catal. Sci. Technol.*, 2025, **15**, 427–434.
122 Q. Zhai, S. Xie, W. Fan, Q. Zhang, Y. Wang, W. Deng and Y. Wang, *Angew. Chem.*, 2013, **125**, 5888–5891.
123 E. Karamian and S. Sharifnia, *J. CO_2 Util.*, 2016, **16**, 194–203.
124 J. Fu, K. Jiang, X. Qiu, J. Yu and M. Liu, *Mater. Today*, 2020, **32**, 222–243.
125 Y. Ji and Y. Luo, *J. Am. Chem. Soc.*, 2016, **138**, 15896–15902.
126 C. F. Shih, T. Zhang, J. Li and C. Bai, *Joule*, 2018, **2**, 1925–1949.
127 A. Dhakshinamoorthy, S. Navalon, A. Corma and H. Garcia, *Energy Environ. Sci.*, 2012, **5**, 9217–9233.
128 M. A. Gondal, A. Lais, M. A. Dastageer, D. Yang, K. Shen and X. Chang, *Int. J. Energy Res.*, 2017, **41**, 2162–2172.
129 S. Ali, R. Iqbal, A. Khan, S. U. Rehman, M. Haneef and L. Yin, *ACS Appl. Nano Mater.*, 2021, **4**, 6893–6902.
130 D. Vadivel, F. Ferraro, D. Merli and D. Dondi, Springer Nature, *Photochem. Photobiol. Sci.*, 2022, **21**, 863–878.
131 M. Q. Yang and Y. J. Xu, *Phys. Chem. Chem. Phys.*, 2013, **15**, 19102–19118.
132 D. C. Grills and E. Fujita, *J. Phys. Chem. Lett.*, 2010, **1**, 2709–2718.
133 X. Li, J. Yu, J. Low, Y. Fang, J. Xiao and X. Chen, *J. Mater. Chem. A*, 2015, **3**, 2485–2534.
134 M. Minella, M. Demontis, M. Sarro, F. Sordello, P. Calza and C. Minero, *J. Mater. Sci.*, 2015, **50**, 2399–2409.
135 K. Spilarewicz-Stanek, A. Jakimińska, A. Kisielewska, M. Dudek and I. Piwoński, *Mater. Sci. Semicond. Process.*, 2021, **123**, 105525.
136 K.-Q. Lu, Y.-H. Li, Z.-R. Tang and Y.-J. Xu, *ACS Mater. Au*, 2021, **1**, 37–54.
137 A. Badoni, S. Thakur, N. Vijayan, H. C. Swart, M. Bechelany, Z. Chen, S. Sun, Q. Cai, Y. Chen and J. Prakash, *Catal. Sci. Technol.*, 2025, **15**, 1702–1770.
138 B. Anegbe, I. H. Ifijen, M. Maliki, I. E. Uwidia and A. I. Aigbodion, *Environ. Sci. Eur.*, 2024, **36**, 15.
139 M. Palomba, G. Carotenuto and A. Longo, *Materials*, 2022, **15**, 6456.
140 L.-Y. Lin, Y. Nie, S. Kavadiya, T. Soundappan and P. Biswas, *Chem. Eng. J.*, 2017, **316**, 449–460.
141 C. B. Hiragond, J. Lee, H. Kim, J.-W. Jung, C.-H. Cho and S.-I. In, *Chem. Eng. J.*, 2021, **416**, 127978.
142 S. Nabil, E. A. Shalaby, M. F. Elkady, Y. Matsushita and A. H. El-Shazly, *Catal. Lett.*, 2022, **152**, 3243–3258.
143 H. Jung, C. Kim, H.-W. Yoo, J. You, J. S. Kim, A. Jamal, I. Gereige, J. W. Ager and H.-T. Jung, *Energy Environ. Sci.*, 2023, **16**, 2869–2878.
144 T. Hisatomi, Q. Wang, F. Zhang, S. Ardo, E. Reisner, H. Nishiyama, A. Kudo, T. Yamada and K. Domen, *Front. Sci.*, 2024, **2**, 1411644.